Bioinformatics approaches to investigate the phytochemicals of *Centella asiatica* against the main protease of SARS-CoV-2

Md. Arif Khan (arif.khan@bge.uoda.edu.bd)
University of Development Alternative https://orcid.org/0000-0002-7329-0366

Md. Abdullah Al Mamun Khan
Mawlana Bhashani Science and Technology University

Shahidur Rahman
Mawlana Bhashani Science and Technology University

Asif Ahsan
Mawlana Bhashani Science and Technology University

Jannatul Maowa Sanjana
Mawlana Bhashani Science and Technology University

Shafi Mahmud
University of Rajshahi, Rajshahi-6205, Bangladesh

A M U B Mahfuz
University of Development Alternative

Ashik Sharfaraz
Mawlana Bhashani Science and Technology University

Mobaidul Islam Khan
Mawlana Bhashani Science and Technology University

Abdullah Al Emran
Melanoma Immunology and Oncology Group, The Centenary Institute, Royal Prince Alfred Hospital, University of Sydney, Camperdown, New South Wales, Australia https://orcid.org/0000-0001-5518-6605

Firoz Ahmed
Noakhali Science and Technology University, Noakhali-3814, Bangladesh https://orcid.org/0000-0002-4781-4736

Mohammad Ali Moni (m.moni@uq.edu.au)
Artificial Intelligence & Digital Health Data Science, School of Health and Rehabilitation Sciences, Faculty of Health and Behavioural Sciences, The University of Queensland, St Lucia, QLD, 4072, Australia https://orcid.org/0000-0003-0756-1006

Research Article

Keywords: SARS-CoV-2, Main Protease, COVID-19, Phytochemicals, Centella asiatica, Molecular Docking, ADMET, Molecular Dynamics

Posted Date: November 22nd, 2021

DOI: https://doi.org/10.21203/rs.3.rs-1099054/v1

Abstract

The recent pandemic caused by the novel coronavirus SARS-CoV-2 has impacted global health by increasing mortality and unexpected infection rate. Extensive clinical research is undergoing to repurposing the old drug against this virus. So, this is an emerging need to develop therapy against the virus. Plant-derived natural products have proven to be potent therapeutics for several infections and diseases. *Centella asiatica*, is a native plant of the Indian subcontinent, has been vastly using as folk medicine against diseases including infectious diseases. So, using bioinformatics approach we identified and checked the phytochemicals of the plant as inhibitors against the main protease (Mpro), the key regulatory enzyme of the SARS-CoV-2 lifecycle. Computer-aided drug designing methods were performed to reveal the best nine drug-like phytochemicals those theoretically have the higher binding affinity of inhibiting Mpro. This outcome may direct to the development of potent therapeutics against the SARS-CoV-2 and demands experimental validation.

Highlights

- Combined computer-aided drug design, virtual high-throughput screening conducted to identify the drug candidate molecules against the main protease of SARS-CoV-2.
- *Centella asiatica* has been used as a traditional herbal therapeutic agent against a wide range of diseases and medical conditions in South Asia for centuries. 107 phytochemicals of this plant have been chosen to check their potentiality as Mpro blockers and found nine lead compounds with excellent drug-like properties against SARS-CoV-2.
- The best nine proposed inhibitors docking energies range from -9 kcal/mol to -9.5 kcal/mol. Those molecules showed excellent hydrogen bond interactions between the lead compounds and the target enzyme. In the ADMET studies, we have found no mutagenic effect, tumorigenic effect, abnormality, and toxicity risk in the reproductive system, carcinogenicity, and AMES toxicity.
- Based on the molecular docking score, the ADMET properties, Molecular Dynamics Simulation, the order of the theoretical drug-like active compounds inhibiting the Mpro is as follows: D1 ≥ D5 ≥ D2 = D8 = D9 ≥ D3 = D4 = D6 = D7.

1. Introduction

Coronaviruses (CoVs) are enveloped viruses containing a single positive-stranded RNA. SARS-CoV-2 is the novel lineage of a group β-coronavirus (Licciardi et al., 2020; Lou et al., 2020; Al-Qahtani, 2020; Wang et al., 2020). The Full length of this novel coronavirus (SARS-CoV-2) genome ranges from 29891 to 29903 nucleotides (nt) long (Zhou et al., 2020; Chen et al., 2020). The disease caused by this novel coronavirus was named COVID-19 (Corona Virus Disease 2019) by World Health Organization (WHO) (Zhou et al., 2020; Gorbalenya et al., 2020). First cases of COVID-19 infection reported in the Wuhan city of Hubei province in China in December 2019. According to WHO in nearly four months, COVID-19 has reached 223 countries, with a record of confirmed cases of 89,048,345 individuals and confirmed the death of

1,930,265 infected people till 12.01.2021. [https://www.who.int/emergencies/diseases/novel-coronavirus-2019]. SARS is categorized as zoonotic diseases as they are transmitted by intermediated hosts, for example, palm civets and dromedary camels (Lu et al., 2020). WHO announced that still there is lacking of evidence about the protection of recovered from COVID-19 from secondary infection having antibodies [https://www.who.int/emergencies/diseases/novel-coronavirus-2019/technical-guidance/critical-preparedness-readiness-and-response-actions-for-covid-19]. Recent reports on immunological responses showed that individuals after SARS-Cov-2 infection do not have a uniformly robust antibody response (Liu et al., 2020). Hence most of the people's naturally occurring immunity after Covid-19 infection is thought to be suboptimal and short-lived and unreliable to achieve herd immunity.

Although the research is progressing to develop new vaccines or therapy against this virus for global mass population, however, currently inadequate quantities of vaccines are available to stop the outbreak and there is no known effective treatment. Therefore, extensive research is ongoing to develop better therapeutics using novel drug discovery approaches (Zhavoronkov et al., 2020). Plant phytochemicals provide a rich resource for computational drug discovery. Many studies targeted plant products as SARS CoV-2 inhibitors and applied computer-aided drug design techniques to find their higher binding affinity. For example, phytochemicals of *Azadirachta indica* (Neem) (Borkotoky and Banerjee, 2020) and alkaloids as well as terpenoids from African medicinal plants (Gyebi et al., 2020) were computationally analyzed while in silico screening, techniques were performed for finding potential inhibitors.

Mpro, being a significant CoV enzyme, can be a potential drug target as it plays a central role in interceding the replication and transcription of the virus (Yoosook et al., 2000; Jin et al., 2020; Anand et al., 2002). Mpro is the main essential enzyme in the viral life cycle that may work with or without the aid of closely related human homologs, making it an attractive target to fight against COVID-19 by antiviral drug designing (Pillaiyar et al., 2016). Plethora of evidence suggested that the herbal remedy of *Centella asiatica* has been used as a therapeutic agent against a wide range of diseases and medical conditions in South Asia for centuries (Brinkhaus et al., 2000; Gohil et al., 2010; Singh et al., 2010). Accumulating experimental proof that in both in vitro and in vivo models suggested that *C. asiatica* exhibits wound healing (Sawatdee et al., 2016), neuroprotective (Gray et al., 2017), antioxidant (Ariffin et al., 2011), anticancer activities (Hafız et al., 2020) and anti-inflammatory effects (Cao et al., 2018). Series of in vitro and in vivo model, preclinical with clinical studies have been carried out with an emphasis on the protective effects of *C. asiatica* against cardiovascular diseases as well as cardiovascular-related clinical conditions like as atherosclerosis, hypertension, hyperlipidemia, hyperglycemia, oxidative stress, and inflammation. Many of these studies found that *C. asiatica* protects against cardiovascular diseases and their related conditions (Razali et al., 2019). In virus inhibition logarithm test to investigate the antiviral efficacy, aqueous extract of *C. asiatica* was showed high antiviral activity to inhibit type 2 herpes simplex virus (HSV-2). Alcohol extracts also showed excellent results (Zheng, 1989). Another study has proved that *C. asiatica* contains active drug like components with intracellular anti-HSV-2 activities (Yoosook et al., 2000). So, we selected *C. asiatica* phytochemicals to find the lead compounds with capabilities to inhibit Mpro. Hence, in computer-aided drug designing and discovery, molecular docking can be the vastly used best alternative in silico technique for finding the binding modes of lead compounds to the target

protein like Mpro of SARS-CoV-2 (Azam et al., 2014; Shushni et al., 2013; Azam et al., 2012; Hossain et al., 2016; Ahmed et al., 2012).

The selective treatment choices are almost impossible as there is no targeted therapeutics against COVID-19 (Yoosook et al., 2000). So, for the sake of finding lead compounds for clinical use, we started combined computer-aided drug design, virtual drug screening, high-throughput screening and molecular dynamics simulation study to identify the lead compounds that can inhibit the COVID-19 virus main protease (Mpro). This study can potentiate the development of better therapeutics against SARS-CoV-2 infection.

2. Materials And Methods

2.1 Retrieval of the structure of SARS-CoV-2 Mpro and phytochemicals list of *C. asiatica*

The human novel coronavirus main protease protein (Mpro) 3D (three-dimensional) crystal structure (accession id- 6LU7) was retrieved from Research Collaboratory for Structural Bioinformatics (RCSB) Protein Data Bank (Berman et al., 2000). Unnecessary objects such as default given ligands and water molecules were removed from the protein data bank (PDB) file (6LU7) using discovery studio 4.5 and PyMOL -2.3.3 (BIOVIA, 2015; Yuan et al.,2017). In case of PyMOL, first it has to be uploaded to the software and then clicked sequence information and found the unnecessary objects during preparation. Then the file was saved as a PDB file format and used for further studies. *Centella asiatica* showed prospective results in many studies against HSV 1 and 2 by itself and/or its compounds. After listing a total of 107 compounds, which are the phytochemicals of *C. asiatica* from the literature (Brinkhaus et al., 2000; Razali et al., 2019; Azerad, 2016; Chandrika and Kumara, 2015; Roy et al., 2013; Zahara et al., 2014; Seevaratnam et al., 2012; Bylka et al., 2014), online database PubChem was searched for 2D structures of the phytochemicals in SDF (Structure Data File) file format (Cheng et al., 2014). Afterwards, the SDFs were converted into 3D structure file PDB by using the Online SMILES Translator and Structure File Generator (Oellien and Nicklaus, 2004). After saving all the SDFs into PDB, the phytochemicals were ready as ligands for docking study with the target Mpro.

2.2. Molecular Docking Simulation

Active site of the Mpro identified before going to molecular docking simulation study through CASTp (http://sts.bioe.uic.edu/castp/index.html?2r7g) and cross checked by another server named metaPocket (https://projects.biotec.tu-dresden.de/metapocket/). In case of CASTp, first the PDB structure of the Mpro has to be uploaded to the server and then clicked calculation to find the active site amino acids of Mpro. Molecular docking simulation was carried out using PyRx 0.8 virtual screening software (Yuliana et al., 2013). For simulating the best interaction, the docking was performed setting the center in axis x- (-26.1601), axis y- 12.5823 and axis z- 59.0673 with the dimension was in axis x- 51.3732 Å, axis y- 66.9737 Å and axis z- 59.6071 Å. After docking simulation, the protein data bank partial charge & atom

type (pdbqt) file format, given by PyRx as output, was saved for further protein-ligand interaction analysis.

2.3. Investigation and visualization of docking simulation result

After docking simulation, PyRx 0.8 was produced with nine possible binding positions as output for each compound. Poses with the highest negative binding free energy (kcal/mol) were selected as the best pose for corresponding ligand binding. After docking simulation was performed, 9(nine) compounds were selected based on docking energy ranking. After that, the best-predicted poses were visualized and analyzed by using Discovery Studio 4.5 and PyMOL -2.3.3 for hydrogen bonding.

2.4. *In silico* ADMET analysis

The ADMET (absorption, distribution, metabolism, excretion, and toxicity) prediction and analysis is the basic step to turn a compound into a drug. This is the process that can generate lead molecules that carries the higher binding affinity to show the satisfying result in ADMET performances in clinical trials. As the ADMET denotes absorption, distribution, metabolism, excretion, and toxicity properties of a drug-like molecule, the prediction and analysis of the ADMET properties of the selected drug-like phytomolecules were performed by the online-based tools. All these ADMET properties were carried out and also compared the results given to all of our selected drug candidates through these 4 mostly used online servers like Molinspiration (Hossain et al., 2016), admetSAR (Yang et al., 2019), SwissADME (Daina et al., 2017), and pkCSM (Pires et al., 2015). The SMILES (Oellien and Nicklaus, 2004) format of the listed phytochemicals of *C. asiatica* were uploaded to those online servers to calculate the ADMET properties and tabulated accordingly.

2.5. Calculation of toxicity potential

Various attributes of the drug-related properties like tumorigenicity, mutagenicity, irritation, reproductive effect, drug-likeness, and drug-score prediction were analyzed using Osiris Property Explorer (Sander, 2001). The SMILES (Oellien and Nicklaus, 2004) format of the drug-like molecules of *C. asiatica* were uploaded to Osiris Property Explorer (Sander, 2001) to calculate the toxicity properties and tabulated accordingly.

2.6. Molecular Dynamics Simulation

The molecular dynamics (MD) simulation of the receptor and epitope complex was carried out through YASARA dynamics (Krieger et al., 2004) tools where AMBER14 force field (Case et al., 2005) was employed. The co-crystalized protein structure was used as a control in this study and, also ligand free apo protein was utilized to compare with nine docked complexes. Initially, the complex was optimized and cleaned and thereafter a cubic simulation cell was created with a box size of (96.0795× 96.0795×96.0795). The cell density of the system was 1.012 gm/cm^3 where TIP3P or (Transferable intermolecular potential 3 points) the model was applied. The periodic boundary condition was maintained. The physiological condition of the simulation system was set as (298K, pH 7.4, 0.9% NaCl)

and the Particle Mesh Ewald method was applied to define long-range electrostatic interaction with a distance of 8Å (Krieger et al., 2006). The initial energy minimization of the system was done through the steepest gradient approach by employing a simulated annealing method. Finally, the molecular dynamics simulation was performed for 50ns and RMSD (Root Mean Square Deviation), RMSF (Root Mean Square Fluctuation), Rg (Radius of Gyration), SASA (Solvent Accessible Surface Area), MM-PBSA (Molecular Mechanics-Poisson Boltzman Surface Area) (Krieger and Vriend, 2015).

3. Result

3.1. Molecular Docking Simulation

The molecular docking analysis performed using PyRx 0.8 for 107 compounds, which are the phytochemicals of *C. asiatica*. PyRx 0.8 produced nine possible binding positions as output for each compound. Out of nine possible ligands binding positions, the best one was chosen for each compound based on the lowest docking energy. From 107 compounds, only 9 compounds were selected based on the binding energy (Figure 1). Amongst the 107 compounds screened, 9 compounds, D1 to D9 (Figure 2), showed the strongest binding energy values with ≤ −9.0 kcal/mol. Based on the binding energy, the 9 compounds, have a very strong binding interaction with Mpro compared to other *C. asiatica* compounds, demonstrating their potential to be used as promising inhibitors. The docking energy values between ligands and proteins shown through hydrogen bonds and hydrophobic bonds as well as their interacting amino acid residues are presented in table 1 and figure 3 and supplementary figure 1. The non-bond interaction distance between amino acids, interaction category, and type of interactions is also displayed in table 2 and supplementary table 1. The anti-SARS-CoV-2 activity of the *C. asiatica* compounds into the Mpro of SARS-CoV-2 was found in the following order: D1 ≥ D5 ≥ D2 = D8 = D9 ≥ D3 = D4 = D6 = D7. The docking energy was negative, in the range of -9.0 to -9.5 kcal/mol (Table 1). Interactions with amino acid included Lys5, Gln127, Cys128, Arg131, Lys137, Thr199, Trp218, Phe219, Arg222, Lys236, Tyr239, Leu271, Leu272, Gly275, Met276, Arg279, Leu282, Leu287, Glu288, Asp289 and Glu290 (Table 1). The docking simulation results are excellent evidence of the anti-SARS-CoV-2 activity of the *C. asiatica* compounds. The highest number of hydrogen bonding interactions was observed in D4 and the lowest number of hydrogen bonding interactions was observed in D2 (Table 1). All compounds showed the conventional hydrogen bond and alkyl bond except the D9 compound. D9 showed the conventional hydrogen bond, carbon-hydrogen bond, alkyl bond, and Pi-Pi-T-shaped bond (Table 2). Detailed molecular interactions of the five lead compounds D1, D2, D5, D8 and D9 (Figure 3 and Table 2), which showed the lowest binding free energies ranging −9.5 to −9.1 kcal/mol, revealed that D1, D2, D5, D8, and D9 formed 9, 4, 6, 6 and 3 conventional hydrogen bond interactions and 5, 4, 1, 5 and 1 alkyl bond respectively while D9 compound formed 2 carbon-hydrogen bond and 1 Pi-Pi-T-shaped bond (Table 2). The most common interacting amino acid residues are Lys 5, Arg 131 and Tyr 239 (Table 1). All three interacting amino acid residues were found in three compounds.

3.2 Pharmacokinetic properties study of drug compounds

A successful oral drug is one which is quickly and completely absorbed from the gastrointestinal tract, distributed specifically to its site of action, metabolized in a way that does not immediately remove its activity, and eliminated properly, without causing any harm to the organs in the body. Because of poor pharmacokinetics (PK) properties, approximately half of all drugs in the development fail to make it (Lipinski et al., 1997). The pharmacokinetics properties such as absorption, distribution, metabolism, excretion, and toxicity (ADMET) have become most important in the selection and improvement process of drug compounds. Therefore, early prediction of ADMET properties has significant contributions that increase the success rate of the *C. asiatica* compounds in future development processes. The pharmacokinetic properties of all the compounds are listed in Tables 3, 4 and 5. Most of the orally administered drugs have a molecular weight is less than 500 and a miLogP (logarithm of partition coefficient) is equal or less than 5. In this study, we found that all compound miLogP value is -1.287 to 1.027 (Table3). For a good oral bioavailability score, the number of the rotatable bond must be ≤ 10 and Topological Polar Surface Area (TPSA) values ≤140 Å² (Veber et al., 2002). In the present study, the number of rotatable bonds of all the compounds is ≤ 10 (Table 3).

Molecular descriptors such as molecular weight, number of H bond donor, number of H bond acceptor, number of rotatable bonds were calculated using admetSAR; TPSA, fraction Csp3, Molar Refractivity were calculated using SwissADME; miLogP and water solubility (LogS) were calculated using Osiris property explorer.

ADMET properties such as Plasma protein binding, 3A4 Substrate, 3A4 inhibitor, 2C9 substrate, 2C9 inhibitor, eye irritation, acute oral toxicity, and honey bee toxicity were calculated using admetSAR. Human intestinal Absorption, Caco-2 permeability, Oral bioavailability, Blood-brain barrier (LogBB), Fraction unbound in plasma, CNS permeability, Volume of distribution (L/kg), Renal OCT2 substrate, Total clearance, Hepatotoxicity, AMES toxicity, Oral Rat Acute Toxicity, Oral Rat Chronic Toxicity and Maximum tolerated dose in human were calculated using pkCSM, In addition, oral bioavailability, lipophilicity, and synthetic accessibility were calculated using SwissADME; GPCR ligand, Ion channel modulator, Kinase inhibitor, Nuclear receptor Ligand, Protease inhibitor, and Enzyme inhibitor were calculated using molinspiration. This is noteworthy that all these essential parameters were found acceptable for the 9 (Nine) predominant *C. asiatica* compounds as potential phytochemicals against the main protease; Mpro of SARS-CoV-2.

3.3 Toxicity risks and drug score assessment

The prediction of the toxicity risks of compounds is much more convenient. In the present study, Osiris property explorer was used to calculate toxicity risk parameters such as mutagenicity, tumorigenicity, irritating effects, and reproductive or developmental toxicity effects of all the *C. asiatica* compound's, D1 to D9 (Table 6). The predictions of these parameters are based on the functional group similarity for the query molecule with the in vitro and in vivo validated compounds present in the database of this online program. The toxicity results can be visualized using color codes; green color shows low toxic tendency whereas red color shows a high tendency of toxicity. In the toxicity, screening results in compound D7

show a high risk of irritation. On the other hand, the rest of the compound has a low risk of toxicity (Table 6).

To assess the *C. asiatica* compound's overall potential to qualify for a drug, the overall drug score was calculated (Table 6), which combines toxicity risk parameters, hydrophobicity (miLogP), water solubility (LogS), molecular weight and drug-likeness of the compound. miLogP values are directly proportional to the oral hydrophobicity of the drug. The more hydrophobic the drug, the higher is the ability of the drug to circulate longer in our body. It would not be easy to excrete such a drug. In the present investigation, the miLogP values of the drug molecules were observed to be in the range of -1.287 to 1.027 (Table 3)

3.4. Molecular Dynamics Simulation analysis

To assess the structural integrity and stability of the protein and ligand complex, molecular dynamics simulation was performed for all nine complexes. The RMSD of the C-alpha atom of the simulated complex revealed that D1, D2, D3, D8, and D9 complex had an initial lower RMSD peak and subsequently reached stability after 10ns (Figure 4). During the whole simulation time, all of the complexes did not exceed 2.5Å value which indicates favorable rigidness and stabilized nature of the complex. On the other hand, the ligand free complex or apo protein and the control complex had a higher RMSD trend than D1, D2, D5, D8, and D9 which confirms the comparatively less flexible nature of the docked complex. However, the D9 complex had a slightly higher RMSD profile than other complexes which indicates less firmness whereas D5 and D1 ensured fewer fluctuations. The supplementary figure S2 also confirmed that D3, D4, D6 had more stability except for D7 where Apo and control exhibited less stability. The Root Mean Square Fluctuation of the simulated system aid to recognize the flexible nature of the amino acid residue. Most of the residues of D1, D2, D3, D8, and D9 confirmed less flexibility which approves the stable nature of the system. The amino acid residue, Ser1, Gly2, Glu47, Gly215, Val303, Thr304, Phe305, and Gln306 exhibited the most flexibility than other residues. Also, the amino acid residue Thr45(beta-turn), Ser46(beta-turn), Glu47(beta-turn), Asp48(beta-turn), Met49(beta-turn), Leu50(beta-turn), Asn51(beta-turn), Pro52(beta-turn), Asn53(beta-turn), Tyr54(helix-strand), Glu55(helix-strand), Asp56(helix-strand), Leu58(helix-strand), Ile59(helix-strand), Arg60(helix-strand) from the Apo protein has more flexibility in beta turn and helix region which reduces in significant degree upon binding with ligand. From the supplementary figure S2, it can be confirmed that the complex D3, D4, D6 and D7 has less flexible amino acid than Apo and control, this structure shows less labile nature, hence indicates the stability. This result along with RMSD value reflects that all docked complexes are more stable and structurally rigid than the control complex.

We also calculated SASA value from the simulation trajectory to understand the change in the surface area. Figure 4 illustrated that, SASA profile did not fluctuate too much for D1 and D5 which approves no significant change in the surface area of these two complexes. However, D2 and D9 had a lower SASA profile from 20 to 30ns which may be responsible for the shrunken of the surface area. Additionally, D8 exhibited a higher trend from 15 to 30ns which indicates the slight expansion of the surface area. The ligand free protein structure initially expands the surface area and from 0 to 18ns and thereafter

stabilized where the control structure had lower SASA value than other complexes during whole simulation time. Although the control complex had contracted nature, lesser deviation in other complexes confirms less change in the protein surface area. Additionally, D3, D4, D6, and D7 had an upper peak from 10 to 20ns and stabilized subsequently (supplementary figure S2). Among the complexes, D4 displayed expansion and slightly flexible nature.

The labile nature and rigidness of the system can be ensured through the radius of gyration. From figure 4, it can be observed that among all five complexes, D1, D5, D8 lower than D2 and D9 which indicates the compact nature of D1, D5, and D8. The control and apo structure did not reveal any significant fluctuation and quite similar trend with D1, D8 and D9 whereas D2 and D5 had an upper Rg profile. However, In case of supplementary figure S2, D6 is less rigid than D3, D4 and D7 as it fluctuates more than those complexes.

The MM-PBSA analysis (Figure 4) showed that the D9 complex displayed more positive energy than D1, D2, D5, and D8 which established better binding of D9 complex than the other four complexes. The complex D2 and D9 had more binding energy than control complex which indicates favorable binding than other complexes. Moreover, the binding energy of D1, D2, and D8 were also found significant and the D5 complex had the lowest binding energy among the five complexes.

In case of Post-MD study, we also found supporting results from molecular dynamics study. The D1 complex had common binding residue in Asp289, Leu287, Asp289, Leu272, Met276 for pre and post-md complex whereas D2 complex had similar binding patterns in Lys137, Tyr239, Leu287, Leu272, Met276 residues. Also, D3 complex shows similar types of interactions with Lys137, Tyr239, Leu287, and Cys128 and also, D4 exhibits the same pattern. Moreover, Lys5, Lys137, Gln127, Glu290, Leu282 conserved for D5 and similar hydrogen bond also found in Thr199, Tyr239, and Asp289 for D6. The pre and post-MD docked complex of D7 stabilized by Lys137, Tyr289, Thr199, Leu287, and Met276 residues. On the other hand, common interactions were observed in Lys5, Thr199, Tyr239, Leu272, Met276, Cys128, Leu287, Tyr289 for D8 where D9 complex also confirmed the conservation of binding dynamics in both post and pre-MD structure (Supplementary Table S2).

4. Discussion

The COVID-19 is affecting severely millions of people and taking thousands of precious lives every day over the globe due to its pandemic behavior making it a winning challenge for the scientific communities across the world for the survival of the human race. But there has been no satisfactory breakthrough yet made in the treatment of COVID-19 (Lake, 2020; Yuen et al., 2020; Fang et al., 2020; Dong et al., 2020). Although some candidate drugs were studied and proposed to treat the disease, the attempts lie ambiguous due to low efficacy (Zhou et al., 2020).

There are several advantages of drugs over vaccines (Gutteridge, 1991; Kremer and Snyder, 2003), a study found moderate evidence of influenza vaccines with mild gastrointestinal events; trivalent inactivated influenza vaccine (TIV) was associated with febrile seizures (Maglione et al., 2014). Moreover,

developing a potent vaccine of RNA viruses are difficult as there always is a challenge to get a strong immune response yet maximal effect in the rise of antigenic changes as RNA viruses are very much prone to rapid mutation thus evolution. Although vaccines are developed targeting epitopes that are strongly conserved, moderately conserved, and poorly conserved antigenic sites in their surface protein, due to mutation these epitopes can be changed causing a serious problem in vaccine designing (Steinhauer and Holland, 1987).

In our current study, molecular docking was applied for high throughput screening and advanced analysis like molecular dynamics of the lead molecules of *C. asiatica* against Mpro of SARS-CoV-2. The coronavirus main protease protein (Mpro) also known as coronavirus 3C-like protease (3CLP) plays the most vital role in controlling viral replication and transcription by performing extensive proteolytic processing of replicase polyproteins, making it a potentially attractive drug target (Zhavoronkov et al., 2020; Wang et al., 2020; Yang et al., 2005). ADMET analysis was done to check the drug and potentiality of the drug candidates inside the human body.

The active site of the main protease revealed a couple of amino acids in its cavity like Lys5, Met6, Thr111, Gln127, Leu282, Glu288, Glu290, Phe291, Asp295, Arg298, and Gln299 with an area of 27.045 and a volume of 5.047. All the *C. asiatica* compounds were performed molecular docking with the main protease of SARS-CoV-2 virus (PDB ID: 6LU7) and nine of them showed good binding energy ranging from -9 Kcal/mol to -9.5 Kcal/mol (Table 1). On the other hand, the known inhibitor N3 (N-[(5-Methylisoxazol-3-YL) Carbonyl] Alanyl-L-Valyl-N~1~-((1R, 2Z) -4-(Benzyloxy)-4-Oxo-1-{[(3R) -2-Oxopyrrolidin-3-YL] Methyl} But-2-Enyl) -L- Leucinamide) showed comparatively less molecular docking energy with the Mpro of SARS-CoV-2 and that was only -6.5 Kcal/mol, indicates the these nine compounds might be better drug candidates. The range of the docking score of the nine lead molecules of the medicinal plant *C. asiatica* has shown greater binding affinity when it was compared to some other plant bioactive compounds studied as inhibitors of the main protease of SARS-CoV-2 in silico. For contrast, in different studies some phytochemicals such as Kaempferol -8.58 Kcal/mol, Quercetin -8.47 Kcal/mol, Luteolin-7-glucoside -8.17 Kcal/mol, Demetoxycurcumine -7.99 Kcal/mol, Naringenin -7.89 Kcal/mol, Apigenine-7-glucoside -7.83 Kcal/mol, Oleuropein -7.31 Kcal/mol, Catechin -7.24 Kcal/mol, Curcumin -7.05 Kcal/mol, Epicatechin-gallate -6.67 Kcal/mol, Zingerol -5.40 Kcal/mol, Gingerol -5.38 Kcal/mol (Khaerunnisa et al., 2020), Nigellicine -5.11696768 Kcal/mol, Nigellidine-6.29734373 Kcal/mol, Carvacrol -4.8290143 Kcal/mol, α-Hederin -5.25583553 Kcal/mol, Thymol -4.50417519 Kcal/mol, Thymoquinone -4.71068573 Kcal/mol (Bouchentouf and Missoum, 2020), 22-Hydroxyhopan-3-one -8.6 Kcal/mol, Chrysopentamine -8.5 Kcal/mol, Normelicopicine -8.1 Kcal/mol, Jozipeltine A -8.0 Kcal/mol, 5,6-Dihydronitidine -7.6 Kcal/mol, 3- Benzoylhosloppone -8.1 Kcal/mol, Cryptobeilic acid C -7.9 Kcal/mol, 6-Acetylswietenolide -7.8 Kcal/mol, (Gyebi et al., 2020), Andrographolide -3.094357 Kcal/mol (Enmozhi et al., 2020), Betulinic acid –4.23 Kcal/mol, Coumaroyltyramine –4.18 Kcal/mol, Cryptotanshinone –6.23 Kcal/mol, Lignan –4.27 Kcal/mol, Sugiol –6.04 Kcal/mol and Tanshinonella –5.02 Kcal/mol (Zhang et al., 2020) has shown lower binding affinity than the lowest score holder (-9 Kcal/mol) lead of our nine lead molecules (Table 1). Meanwhile, some leads had a similar binding affinity, for instance, 6-Oxoisoiguesterin -9.1 Kcal/mol, Cryptospirolepine -9.2 Kcal/mol, and 10-Hydroxyusambarensine -10.0

Kcal/mol, Cryptoquindoline -9.7 Kcal/mol were found to have greater binding affinity than the nine *C. asiatica* leads (Gyebi et al., 2020).

Some recently conducted studies have investigated the binding affinities of some repurposed proposed drugs and FDA approved drug compounds as SARS-CoV-2 main protease inhibitors and in comparison with our studied nine lead phytochemicals of *C. asiatica*, they have shown to have lesser binding affinities. For instance, Lopinavir -4.1 kcal/mol, Oseltamivir -4.65 kcal/mol, Ritonavir -5.11 kcal/mol (Muralidharan et al., 2020), Disulfiram -4.0 kcal/mol, Captopril -4.7 kcal/mol, N,Ndiethyldithiocarbamate -2.7 kcal/mol, MeDDTC sulfide -2.9 kcal/mol, MeDDTC sulfoxide -3.5 kcal/mol, MeDDTC sulfone -3.8 kcal/mol, MeDTC sulfoxide -3.2 kcal/mol, MeDTC sulfone -4.3 kcal/mol (Lobo-Galo et al., 2020), Chloroquine -6.2930522 kcal/mol, Hydroxychloroquine -5.57386112 kcal/mol, Azythromycine -5.57062292 kcal/mol, Arbidol -7.15007734 kcal/mol, Remdesivir -6.35291243 kcal/mol and Favipiravir -4.23310471 kcal/mol (Bouchentouf and Missoum, 2020). Some studies specifically investigated the binding affinity of some antiviral compounds as SARS-CoV-2 main protease inhibitors. And the scores were Aloe-emodin -7.4 kcal/mol, Withaferin A -7.7 kcal/mol, Withanolide D -7.8 kcal/mol, Nelfinavir -8.4 kcal/mol, Rhein -8.1, Enoxacin -7.4 kcal/mol, Chitranone -7.0 kcal/mol, Chrysophanol -7.0 kcal/mol, Diterpene -7.1 kcal/mol, Elliptinone -6.9 kcal/mol, Emetine -7.0 kcal/mol and Imatinib -7.4 kcal/mol (Kumar et al., 2020), relatively lower than the nine *C. asiatica* leads scores we found.

When it comes to comparing the study of hydrogen (H) bonds formation, Khaerunnisa et al achieved 3 to 8 H bonds (Khaerunnisa et al., 2020), Bouchentouf and Missoum achieved the number of H bonds was 0-3 (Bouchentouf and Missoum, 2020), Gyebi et al's study achieved the number of H bonds was 0-1 (Gyebi et al., 2020), Enmozhi et al found 4 H bonds (Enmozhi et al., 2020), and finally, Lobo-Galo et al study achieved the number of H bonds was 0 to 5 (Lobo-Galo et al., 2020) but on the other hand in our study, we got 4 to 11 hydrogen bonds formed between the lead compounds and the target enzyme Mpro (Table 1).

We got incredible results when we compared the logP values and logS values of our lead compounds with similar computational drug designing studies done by others. In a previous study, Bouchentouf and Missoum showed logP value was 1.06 to 3.52, and logS value was -8.24 to -2.01 (Bouchentouf and Missoum, 2020), Gyebi et al showed ClogP value was 3.31 to 4.80 (Gyebi et al., 2020). We have found that the miLogP value is -1.287 to 1.027 and logs value is - 5.319 to - 4.073 in our study (Table 3). Gyebi et al showed the bioavailability score was 0.55, non-AMES toxic, and non-carcinogens (Gyebi et al., 2020) whereas in our study the bioavailability score is 0.17 to 0.55 and all the target compounds are non-AMES toxic and non-carcinogens. The acute oral rat toxicity (LD50) was found to be 2.162 mol/kg and Chronic oral rat toxicity (LOAEL) was found to be 1 log mg/ kg_bw/day (Enmozhi et al., 2020). In our study, the acute oral rat toxicity (LD50) is 2.656 to 3.452 mol/kg and chronic oral rat toxicity (LOAEL) is 1.911 to 3.846 log mg/ kg_bw/day (Table 4).

When it comes to cytotoxicity or side effect studies, our proposed compounds show excellent results in *in silico* prediction. In a study, *C. asiatica* was found as a causative factor in abnormality in reproduction

such as infertility in mice and abortion in women in chronic treatment (Orhan, 2012) but the plant *C. asiatica* phytochemicals we have worked with, Osiris property explorer showed no predictions of any abnormalities or toxicity risk in the reproductive system. Moreover, no prediction of any mutagenic effect and the tumorigenic effect was found although one compound showed an irritating effect (Table 6). The pharmacokinetic properties of the selected molecules were carried out by using online-based software tools. All the lead compounds tested in our study showed a moderate to the high absorption rate. Compound D1 showed a high absorption rate of 100% whereas compound D4 showed the lowest absorption in 25.448%. All compounds are the substrate of CYP3A4 and no carcinogenicity and AMES toxicity are present in the prediction (Table 4).

ADME and toxicity analysis of these compounds suggest that they could be used for the development of new drugs to treat COVID-19 although further validation is necessary. MD simulation is an imperative method to explore the protein-ligand complex in real-time, widely used to assess the conformational variability and stability of the protein systems (Mahmud et al., 2020; Bappy et al., 2020; Islam et al., 2019). The molecular dynamics simulation represents stable RMSD compared to ligand free apo structure and control which provides insights about the structural integrity of the docked complex (Dash et al., 2019; Arifuzzaman et al., 2020). Furthermore, Rg profile was illustrated along with RMSD profile, where RMSD describes the fluctuation during simulation periods, and protein folding and degree of compactness describes through Rg. The RMSD and RMSF profile of all 9 systems confirms the rigidness and less flexibility. Moreover, post-MD binding interaction analysis supports the findings from molecular dynamics simulation as almost every hydrogen and hydrophobic bond remains in rigid in post-MD docked complex. After MD analysis, we have also superimposed all the molecular docking complexes and found a structural similarity to them with the previous complexes (Figure S3). Furthermore, we analyzed the hydrogen bond stability from the molecular dynamics simulation trajectory. The supplementary figure S4 demonstrated that most of the complex has more hydrogen bonds than the control complex. However, complex D4, D5, and D6 have more hydrogen bonds than other complexes which indicate the comparative stability of the complex. When it comes to molecular docking, Out of nine drug candidates, D1 showed slightly higher energy than others. However, in the case of ADMET properties in the human body, D9 expressed the best hit although D1 showed the highest absorption, out of those nine compounds. When it comes to molecular dynamics, D1, D2, D5, D8, and D9 showed more suitability as a candidate drug rather than D3, D4, D6, and D7. However, MM-PBSA analysis revealed that the D9 complex demonstrated the most favorable binding than other complexes. This study is limited to in silico modeling and analysis of the bioactive compound of *C. asiatica* against COVID-19. Hence experimental validation is fundamental to assess the efficacy of the selected bioactive compounds.

5. Conclusion

Overall our *in silico* drug designing findings revealed nine potential phytochemicals from the bioactive compounds of *C. asiatica against* SARS-COV-2 replication and propagation associated protein- Main Protease. Based on our comprehensive computational molecular docking, pharmacokinetics study, molecular dynamics simulation, we have identified nine phytochemicals of C. *asiatica* exhibited

enhanced binding affinities to target the main-protease of SARS-CoV-2 compared to approved anti-viral drugs. Most importantly, the proposed compound is also predicted to less likely to have side-effects in patients. The main advantage to use the phytochemicals of *C. asiatica*, it is readily available and has been used as a traditional medicine in many regions of Asia including India and China. Since vaccine development against SARS-CoV-2 requires a considerable amount of time, therefore, our proposed bioactive compounds of *C. asiatica* could be a potential alternative therapy against this deadly virus.

The accumulative findings of our study make a stronger case which demands future studies to investigate the possible preclinical and clinical efficacy of these agents' efficient treatment of SARS-CoV-2.

Declarations

Acknowledgments

None to acknowledge.

Funding

No funding was obtained for this work.

Authors Contribution

MAK, MAM: Conceptualization and Design; Methodology; Data curation; Critical Analysis; Writing - review & editing. **MAMK, SR:** Formal analysis; Software and Server Use; Writing - original draft. **AA, JMS:** Docking Study; Software and Server Use; Visualization; **SM:** Molecular Dynamics study; Visualization**;** Writing - review & editing. **AMUBM,AS, MIK:** Software and Server Use; Visualization; **AAE, FA:** Validation; Critical Analysis, Writing - review & editing.

Declaration of Interests

The other authors have no competing interests.

References

Ahmed, M. A., Azam, F., Rghigh, A. M., Gbaj, A., & Zetrini, A. E. (2012). Structure-based design, synthesis, molecular docking, and biological activities of 2-(3-benzoylphenyl) propanoic acid derivatives as dual mechanism drugs. *Journal of pharmacy & bioallied sciences*, *4*(1), 43.

Al-Qahtani, A. A. (2020). Severe acute respiratory syndrome coronavirus 2 (SARS-CoV-2): emergence, History, Basic and Clinical Aspects. *Saudi journal of biological sciences*.

Anand, K., Palm, G. J., Mesters, J. R., Siddell, S. G., Ziebuhr, J., & Hilgenfeld, R. (2002). Structure of coronavirus main proteinase reveals combination of a chymotrypsin fold with an extra α-helical domain.

The EMBO journal, *21*(13), 3213-3224.

Ariffin, F., Heong Chew, S., Bhupinder, K., Karim, A. A., & Huda, N. (2011). Antioxidant capacity and phenolic composition of fermented Centella asiatica herbal teas. *Journal of the Science of Food and Agriculture*, *91*(15), 2731-2739.

Arifuzzaman, M., Hamza, A., Zannat, S. S., Fahad, R., Rahman, A., Hosen, S. Z., ... & Hossain, M. K. (2020). Targeting galectin-3 by natural glycosides: a computational approach. *Network Modeling Analysis in Health Informatics and Bioinformatics*, *9*(1), 1-15.

Azam, F., Amer, A. M., Abulifa, A. R., & Elzwawi, M. M. (2014). Ginger components as new leads for the design and development of novel multi-targeted anti-Alzheimer's drugs: a computational investigation. *Drug design, development and therapy*, *8*, 2045.

Azam, F., Vijaya Vara Prasad, M., Thangavel, N., Kumar Shrivastava, A., & Mohan, G. (2012). Structure-based design, synthesis and molecular modeling studies of thiazolyl urea derivatives as novel anti-parkinsonian agents. *Medicinal Chemistry*, *8*(6), 1057-1068.

Azerad, R. (2016). Chemical structures, production and enzymatic transformations of sapogenins and saponins from Centella asiatica (L.) Urban. *Fitoterapia*, *114*, 168-187.

Bappy, S. S., Sultana, S., Adhikari, J., Mahmud, S., Khan, M. A., Kibria, K. K., ... & Shibly, A. Z. (2020). Extensive Immunoinformatics study for the prediction of novel peptide-based epitope vaccine with docking confirmation against Envelope protein of Chikungunya virus: A Computational Biology Approach. *Journal of Biomolecular Structure and Dynamics*, 1-16.

Berman, H. M., Westbrook, J., Feng, Z., Gilliland, G., Bhat, T. N., Weissig, H., ... & Bourne, P. E. (2000). The protein data bank. *Nucleic acids research*, *28*(1), 235-242.

BIOVIA, D. S. (2015). BIOVIA Discovery Studio Visualizer, v16. 1.0. 15350. *San Diego: Dassault Systèmes*.

Borkotoky, S., & Banerjee, M. (2020). A computational prediction of SARS-CoV-2 structural protein inhibitors from Azadirachta indica (Neem). *Journal of Biomolecular Structure and Dynamics*, 1-11.

Bouchentouf, S., & Missoum, N. (2020). Identification of compounds from Nigella sativa as new potential inhibitors of 2019 novel Coronasvirus (COVID-19): Molecular docking study.

Brinkhaus, B., Lindner, M., Schuppan, D., & Hahn, E. G. (2000). Chemical, pharmacological and clinical profile of the East Asian medical plant Centella aslatica. *Phytomedicine*, *7*(5), 427-448.

Bylka, W., Znajdek-Awiżeń, P., Studzińska-Sroka, E., Dańczak-Pazdrowska, A., & Brzezińska, M. (2014). Centella asiatica in dermatology: an overview. *Phytotherapy research*, *28*(8), 1117-1124.

Cao, S. Y., Wang, W., Nan, F. F., Liu, Y. N., Wei, S. Y., Li, F. F., & Chen, L. (2018). Asiatic acid inhibits LPS-induced inflammatory response in endometrial epithelial cells. *Microbial pathogenesis*, *116*, 195-199.

Case, D. A., Cheatham III, T. E., Darden, T., Gohlke, H., Luo, R., Merz Jr, K. M., ... & Woods, R. J. (2005). The Amber biomolecular simulation programs. *Journal of computational chemistry*, *26*(16), 1668-1688.

Chandrika, U. G., & Kumara, P. A. P. (2015). Gotu kola (Centella asiatica): nutritional properties and plausible health benefits. *Advances in food and nutrition research*, *76*, 125-157.

Chen, L., Liu, W., Zhang, Q., Xu, K., Ye, G., Wu, W., ... & Liu, Y. (2020). RNA based mNGS approach identifies a novel human coronavirus from two individual pneumonia cases in 2019 Wuhan outbreak. *Emerging microbes & infections*, *9*(1), 313-319.

Cheng, T., Pan, Y., Hao, M., Wang, Y., & Bryant, S. H. (2014). PubChem applications in drug discovery: a bibliometric analysis. *Drug discovery today*, *19*(11), 1751-1756.

Daina, A., Michielin, O., & Zoete, V. (2017). SwissADME: a free web tool to evaluate pharmacokinetics, drug-likeness and medicinal chemistry friendliness of small molecules. *Scientific reports*, *7*(1), 1-13.

Dash, R., Ali, M., Dash, N., Azad, M., Kalam, A., Hosen, S. M., ... & Moon, I. S. (2019). Structural and dynamic characterizations highlight the deleterious role of SULT1A1 R213H polymorphism in substrate binding. *International journal of molecular sciences*, *20*(24), 6256.

Dong, L., Hu, S., & Gao, J. (2020). Discovering drugs to treat coronavirus disease 2019 (COVID-19). *Drug discoveries & therapeutics*, *14*(1), 58-60.

Enmozhi, S. K., Raja, K., Sebastine, I., & Joseph, J. (2020). Andrographolide as a potential inhibitor of SARS-CoV-2 main protease: An in silico approach. *Journal of Biomolecular Structure and Dynamics*, 1-7.

Fang, Y. (2020). Fang Y, Zhang H, Xie J, et al. *Sensitivity of chest CT for COVID-19: comparison to RT-PCR. Radiology*, *200432*.

Gohil, K. J., Patel, J. A., & Gajjar, A. K. (2010). Pharmacological review on Centella asiatica: a potential herbal cure-all. *Indian journal of pharmaceutical sciences*, *72*(5), 546.

Gorbalenya, A. E., Baker, S. C., Baric, R., Groot, R. J. D., Drosten, C., Gulyaeva, A. A., ... & Ziebuhr, J. (2020). Severe acute respiratory syndrome-related coronavirus: The species and its viruses–a statement of the Coronavirus Study Group.

Gray, N. E., Zweig, J. A., Matthews, D. G., Caruso, M., Quinn, J. F., & Soumyanath, A. (2017). Centella asiatica attenuates mitochondrial dysfunction and oxidative stress in Aβ-exposed hippocampal neurons. *Oxidative medicine and cellular longevity*, *2017*.

Gutteridge, W. E. (1991). Control of parasitic diseases: a complementary role for vaccines and drugs. *Immunology letters*, *30*(2), 261-265.

Gyebi, G. A., Ogunro, O. B., Adegunloye, A. P., Ogunyemi, O. M., & Afolabi, S. O. (2020). Potential inhibitors of coronavirus 3-chymotrypsin-like protease (3CLpro): An in silico screening of alkaloids and terpenoids from African medicinal plants. *Journal of Biomolecular Structure and Dynamics*, 1-13.

Hafiz, Z. Z., Amin, M., Johari James, R. M., Teh, L. K., Salleh, M. Z., & Adenan, M. I. (2020). Inhibitory effects of Raw-Extract Centella Asiatica (RECA) on Acetylcholinesterase, Inflammations, and oxidative stress activities via in vitro and in vivo. *Molecules*, *25*(4), 892.

Hossain, M. U., Khan, M., Rakib-Uz-Zaman, S. M., Ali, M. T., Islam, M., Keya, C. A., & Salimullah, M. (2016). Treating diabetes mellitus: pharmacophore based designing of potential drugs from Gymnema sylvestre against insulin receptor protein. *BioMed research international*, *2016*.

Hossain, M. U., Oany, A. R., Ahmad, S. A. I., Hasan, M. A., Khan, M. A., & Siddikey, M. A. A. (2016). Identification of potential inhibitor and enzyme-inhibitor complex on trypanothione reductase to control Chagas disease. *Computational biology and chemistry*, *65*, 29-36.

Islam, M. J., Parves, M. R., Mahmud, S., Tithi, F. A., & Reza, M. A. (2019). Assessment of structurally and functionally high-risk nsSNPs impacts on human bone morphogenetic protein receptor type IA (BMPR1A) by computational approach. *Computational biology and chemistry*, *80*, 31-45.

Jin, Z., Du, X., Xu, Y., Deng, Y., Liu, M., Zhao, Y., ... & Yang, H. (2020). Structure of M pro from SARS-CoV-2 and discovery of its inhibitors. *Nature*, *582*(7811), 289-293.

Khaerunnisa, S., Kurniawan, H., Awaluddin, R., Suhartati, S., & Soetjipto, S. (2020). Potential inhibitor of COVID-19 main protease (Mpro) from several medicinal plant compounds by molecular docking study.

Kremer, M., & Snyder, C. M. (2003). *Why are drugs more profitable than vaccines?* (No. w9833). National Bureau of Economic Research.

Krieger, E., & Vriend, G. (2015). New ways to boost molecular dynamics simulations. *Journal of computational chemistry*, *36*(13), 996-1007.

Krieger, E., Darden, T., Nabuurs, S. B., Finkelstein, A., & Vriend, G. (2004). Making optimal use of empirical energy functions: force-field parameterization in crystal space. *Proteins: Structure, Function, and Bioinformatics*, *57*(4), 678-683.

Krieger, E., Nielsen, J. E., Spronk, C. A., & Vriend, G. (2006). Fast empirical pKa prediction by Ewald summation. *Journal of molecular graphics and modelling*, *25*(4), 481-486.

Kumar, D., Chandel, V., Raj, S., & Rathi, B. (2020). In silico identification of potent FDA approved drugs against Coronavirus COVID-19 main protease: A drug repurposing approach. *Chemical Biology Letters*,

7(3), 166-175.

Lake, M. A. (2020). What we know so far: COVID-19 current clinical knowledge and research. *Clinical Medicine*, *20*(2), 124.

Licciardi, F., Giani, T., Baldini, L., Favalli, E. G., Caporali, R., & Cimaz, R. (2020). COVID-19 and what pediatric rheumatologists should know: a review from a highly affected country. *Pediatric Rheumatology*, *18*, 1-7.

Lipinski, C. A., Lombardo, F., Dominy, B. W., & Feeney, P. J. (1997). Experimental and computational approaches to estimate solubility and permeability in drug discovery and development settings. *Advanced drug delivery reviews*, *23*(1-3), 3-25.

Liu, T., Wu, S., Tao, H., Zeng, G., Zhou, F., Guo, F., & Wang, X. (2020). Prevalence of IgG antibodies to SARS-CoV-2 in Wuhan-implications for the ability to produce long-lasting protective antibodies against SARS-CoV-2. *MedRxiv*.

Lobo-Galo, N., Terrazas-López, M., Martínez-Martínez, A., & Díaz-Sánchez, Á. G. (2020). FDA-approved thiol-reacting drugs that potentially bind into the SARS-CoV-2 main protease, essential for viral replication. *Journal of Biomolecular Structure and Dynamics*, 1-9.

Lou, J., Tian, S. J., Niu, S. M., Kang, X. Q., Lian, H. X., Zhang, L. X., & Zhang, J. J. (2020). Coronavirus disease 2019: a bibliometric analysis and review. *Eur Rev Med Pharmacol Sci*, *24*(6), 3411-21.

Lu, R., Zhao, X., Li, J., Niu, P., Yang, B., Wu, H., ... & Tan, W. (2020). Genomic characterisation and epidemiology of 2019 novel coronavirus: implications for virus origins and receptor binding. *The lancet*, *395*(10224), 565-574.

Maglione, M. A., Das, L., Raaen, L., Smith, A., Chari, R., Newberry, S., ... & Gidengil, C. (2014). Safety of vaccines used for routine immunization of US children: a systematic review. *Pediatrics*, *134*(2), 325-337.

Mahmud, S., Parves, M. R., Riza, Y. M., Sujon, K. M., Ray, S., Tithi, F. A., ... & Absar, N. (2020). Exploring the potent inhibitors and binding modes of phospholipase A2 through in silico investigation. *Journal of Biomolecular Structure and Dynamics*, *38*(14), 4221-4231.

Muralidharan, N., Sakthivel, R., Velmurugan, D., & Gromiha, M. M. (2020). Computational studies of drug repurposing and synergism of lopinavir, oseltamivir and ritonavir binding with SARS-CoV-2 protease against COVID-19. *Journal of Biomolecular Structure and Dynamics*, 1-6.

Oellien, F., & Nicklaus, M. C. (2004). Online SMILES translator and structure file generator.

Orhan, I. E. (2012). Centella asiatica (L.) Urban: from traditional medicine to modern medicine with neuroprotective potential. *Evidence-based complementary and alternative medicine*, *2012*.

Pillaiyar, T., Manickam, M., Namasivayam, V., Hayashi, Y., & Jung, S. H. (2016). An overview of severe acute respiratory syndrome–coronavirus (SARS-CoV) 3CL protease inhibitors: peptidomimetics and small molecule chemotherapy. *Journal of medicinal chemistry*, *59*(14), 6595-6628.

Pires, D. E., Blundell, T. L., & Ascher, D. B. (2015). pkCSM: predicting small-molecule pharmacokinetic and toxicity properties using graph-based signatures. *Journal of medicinal chemistry*, *58*(9), 4066-4072.

Razali, N. N. M., Ng, C. T., & Fong, L. Y. (2019). Cardiovascular protective effects of Centella asiatica and its triterpenes: a review. *Planta medica*, *85*(16), 1203-1215.

Roy, D. C., Barman, S. K., & Shaik, M. M. (2013). Current updates on Centella asiatica: phytochemistry, pharmacology and traditional uses. *Medicinal Plant Research*, *3*.

Sander, T. (2001). OSIRIS property explorer. *Organic Chemistry Portal*.

Sawatdee, S., Choochuay, K., Chanthorn, W., & Srichana, T. (2016). Evaluation of the topical spray containing Centella asiatica extract and its efficacy on excision wounds in rats. *Acta Pharmaceutica*, *66*(2), 233-244.

Seevaratnam, V., Banumathi, P., Premalatha, M. R., Sundaram, S. P., & Arumugam, T. (2012). Functional properties of Centella asiatica (L.): a review. *Int J Pharm Pharm Sci*, *4*(5), 8-14.

Shushni, M. A. M., Azam, F., & Lindequist, U. (2013). Oxasetin from Lophiostoma sp. of the Baltic Sea: identification, in silico binding mode prediction and antibacterial evaluation against fish pathogenic bacteria. *Natural product communications*, *8*(9), 1934578X1300800909.

Singh, S., Gautam, A., Sharma, A., & Batra, A. (2010). Centella asiatica (L.): a plant with immense medicinal potential but threatened. *International journal of pharmaceutical sciences review and research*, *4*(2), 9-17.

Steinhauer, D. A., & Holland, J. J. (1987). Rapid evolution of RNA viruses. *Annual Reviews in Microbiology*, *41*(1), 409-431.

Veber, D. F., Johnson, S. R., Cheng, H. Y., Smith, B. R., Ward, K. W., & Kopple, K. D. (2002). Molecular properties that influence the oral bioavailability of drug candidates. *Journal of medicinal chemistry*, *45*(12), 2615-2623.

Wang, Q., Zhao, Y., Chen, X., & Hong, A. (2020). Virtual screening of approved clinic drugs with main protease (3CLpro) reveals potential inhibitory effects on SARS-CoV-2. *Journal of Biomolecular Structure and Dynamics*, 1-11.

Wang, Y., Wang, Y., Chen, Y., & Qin, Q. (2020). Unique epidemiological and clinical features of the emerging 2019 novel coronavirus pneumonia (COVID-19) implicate special control measures. *Journal of medical virology*, *92*(6), 568-576.

Yang, H., Lou, C., Sun, L., Li, J., Cai, Y., Wang, Z., ... & Tang, Y. (2019). admetSAR 2.0: web-service for prediction and optimization of chemical ADMET properties. *Bioinformatics*, *35*(6), 1067-1069.

Yang, H., Xie, W., Xue, X., Yang, K., Ma, J., Liang, W., ... & Rao, Z. (2005). Design of wide-spectrum inhibitors targeting coronavirus main proteases. *PLoS Biol*, *3*(10), e324.

Yoosook, C., Bunyapraphatsara, N., Boonyakiat, Y., & Kantasuk, C. (2000). Anti-herpes simplex virus activities of crude water extracts of Thai medicinal plants. *Phytomedicine*, *6*(6), 411-419.

Yuan, S., Chan, H. S., & Hu, Z. (2017). Using PyMOL as a platform for computational drug design. *Wiley Interdisciplinary Reviews: Computational Molecular Science*, *7*(2), e1298.

Yuen, K. S., Ye, Z. W., Fung, S. Y., Chan, C. P., & Jin, D. Y. (2020). SARS-CoV-2 and COVID-19: The most important research questions. *Cell & bioscience*, *10*(1), 1-5.

Yuliana, D., Bahtiar, F. I., & Najib, A. (2013). In silico screening of chemical compounds from roselle (Hibiscus Sabdariffa) as angiotensin-I converting enzyme inhibitor used PyRx program. *ARPN J. Sci. Technol*, *3*, 1158-1160.

Zahara, K., Bibi, Y., & Tabassum, S. (2014). Clinical and therapeutic benefits of Centella asiatica. *Pure and Applied Biology*, *3*(4), 152.

Zhang, D. H., Wu, K. L., Zhang, X., Deng, S. Q., & Peng, B. (2020). In silico screening of Chinese herbal medicines with the potential to directly inhibit 2019 novel coronavirus. *Journal of integrative medicine*, *18*(2), 152-158.

Zhavoronkov, A., Aladinskiy, V., Zhebrak, A., Zagribelnyy, B., Terentiev, V., Bezrukov, D. S., ... & Ivanenkov, Y. (2020). Potential COVID-2019 3C-like protease inhibitors designed using generative deep learning approaches. *Insilico Medicine Hong Kong Ltd A*, *307*, E1.

Zheng, M. S. (1989). An experimental study of the anti-HSV-II action of 500 herbal drugs. *Journal of traditional Chinese medicine= Chung i tsa chih ying wen pan*, *9*(2), 113-116.

Zhou, D., Dai, S. M., & Tong, Q. (2020). COVID-19: a recommendation to examine the effect of hydroxychloroquine in preventing infection and progression. *Journal of Antimicrobial Chemotherapy*, *75*(7), 1667-1670.

Zhou, P., Yang, X. L., Wang, X. G., Hu, B., Zhang, L., Zhang, W., ... & Shi, Z. L. (2020). A pneumonia outbreak associated with a new coronavirus of probable bat origin. *nature*, *579*(7798), 270-273.

Tables

Table 1: Binding energy (kcal/mol) and non-bonding interactions of a different lead compound against SARS-CoV-2 Mpro.

Compounds	Binding Energy (kcal/mol)	Hydrogen bond Interaction		Hydrophobic interaction	
		No. of bonds	Residues involved	No. of bonds	Residues involved
D1	-9.5	9	Lys5, Gln127, Arg131, Lys236, Tyr239, Asp289, Glu290	5	Cys128, Leu272, Met276, Leu287
D2	-9.1	4	Lys137, Thr199, Lys236, Tyr239	4	Leu272, Met276, Leu287
D3	-9	6	Lys5, Gln127, Thr199, Tyr239, Glu290	5	Cys128, Leu272, Met276, Leu287
D4	-9	11	Lys5, Gln127, Arg131, Lys137, Thr199, Lys236, Tyr239, Leu271, Glu288, Glu290	3	Cys128, Leu272, Leu287
D5	-9.2	6	Lys5, Gln127, Arg131, Leu282, Glu290	1	Lys137
D6	-9	6	Lys5, Arg131, Thr199, Lys236, Tyr239, Asp289	5	Cys128, Leu272, Met276, Leu287
D7	-9	8	Lys5, Arg131, Lys137, Thr199, Lys236, Tyr239, Glu290	5	Cys128, Leu272, Met276, Leu287
D8	-9.1	6	Lys5, Arg131, Thr199, Tyr239, Asp289	5	Cys128, Leu272, Met276, Leu287
D9	-9.1	5	Arg222, Arg279, Phe219, Gly275	2	Trp218, Leu271

Table 2: Molecular non-bond interactions of the lead compounds with SARS-CoV-2 Mpro.

Compounds	Binding Energy (kcal/mol)	Interacting amino acid residues	Bond distance (Å)	Interaction category	Type of Interaction
D1	-9.5	Lys5	3.24108	H Bond	Conventional H Bond
		Gln127	2.45974	H Bond	Conventional H Bond
		Arg131	2.96429	H Bond	Conventional H Bond
		Lys236	3.26263	H Bond	Conventional H Bond
		Lys236	2.37931	H Bond	Conventional H Bond
		Tyr239	3.128	H Bond	Conventional H Bond
		Asp289	2.73836	H Bond	Conventional H Bond
		Asp289	2.54557	H Bond	Conventional H Bond
		Glu290	2.23055	H Bond	Conventional H Bond
		Cys128	4.22317	Hy	Alkyl
		Leu272	4.63235	Hy	Alkyl
		Met276	4.73592	Hy	Alkyl
		Leu287	4.88206	Hy	Alkyl
		Leu287	4.35754	Hy	Alkyl
D2	-9.1	Lys137	3.36992	H Bond	Conventional H Bond
		Thr199	2.73408	H Bond	Conventional H Bond
		Lys236	3.23523	H Bond	Conventional H Bond
		Tyr239	3.1467	H Bond	Conventional H Bond
		Leu272	4.64594	Hy	Alkyl
		Met276	4.81827	Hy	Alkyl
		Leu287	4.89975	Hy	Alkyl

		Leu287	4.42611	Hy	Alkyl
D5	-9.2	Lys5	2.87175	H Bond	Conventional H Bond
		Gln127	2.245	H Bond	Conventional H Bond
		Arg131	3.19792	H Bond	Conventional H Bond
		Leu282	2.70342	H Bond	Conventional H Bond
		Leu282	2.11691	H Bond	Conventional H Bond
		Glu290	2.30022	H Bond	Conventional H Bond
		Lys137	4.91546	Hy	Alkyl
D8	-9.1	Lys5	3.09536	H Bond	Conventional H Bond
		Lys5	3.21636	H Bond	Conventional H Bond
		Arg131	2.91577	H Bond	Conventional H Bond
		Thr199	2.7578	H Bond	Conventional H Bond
		Tyr239	3.11225	H Bond	Conventional H Bond
		Asp289	2.85852	H Bond	Conventional H Bond
		Cys128	4.19893	Hy	Alkyl
		Leu272	4.67051	Hy	Alkyl
		Met276	4.74128	Hy	Alkyl
		Leu287	4.91341	Hy	Alkyl
		Leu287	4.37864	Hy	Alkyl
		Arg222	3.04796	H Bond	Conventional H Bond
		Arg222	3.095	H Bond	Conventional H Bond

D9	-9.1	Arg279	2.89344	H Bond	Conventional H Bond
		Phe219	3.78449	H Bond	Carbon H Bond
		Gly275	3.29564	H Bond	Carbon H Bond
		Trp218	5.64116	Hy	Pi-Pi-T-shaped
		Leu271	4.77661	Hy	Alkyl

H= Hydrogen, Hy= Hydrophobic

Table 5: Bioactivity score of the selected compound.

Compounds	GPCR ligand	Ion channel modulator	Kinase inhibitor	Nuclear receptor ligand	Protease inhibitor	Enzyme inhibitor
D1	-3.25	-3.67	-3.68	-3.52	-2.81	-3.16
D2	-1.60	-2.96	-2.69	-2.17	-1.06	-1.70
D3	-3.25	-3.66	-3.67	-3.53	-2.83	-3.15
D4	-3.46	-3.72	-3.71	-3.59	-3.08	-3.36
D5	-3.33	-3.68	-3.70	-3.54	-2.95	-3.21
D6	-3.37	-3.68	-3.70	-3.55	-2.95	-3.23
D7	-3.45	-3.69	-3.72	-3.59	-3.00	-3.33
D8	-3.38	-3.70	-3.70	-3.55	-2.96	-3.26
D9	0.18	-0.11	-0.45	0.45	0.06	0.34

Table 6: Drug-likeness/scores and toxicity calculations of *Centella asiatica* compounds based on Osiris property explorer

Compound	Solubility	Drug - likeness	Mutagenic	Tumorigenic	Irritant	Reproductive effect	Drug score
D1	-5.319	-10.698	Green	Green	Green	Green	0.177
D2	-4.605	-8.04	Green	Green	Green	Green	0.203
D3	-5.211	-12.636	Green	Green	Green	Green	0.18
D4	-4.305	-13.892	Green	Green	Green	Green	0.208
D5	-4.92	-10.698	Green	Green	Green	Green	0.19
D6	-4.584	-12.292	Green	Green	Green	Green	0.2
D7	-5.297	-11.506	Green	Green	Red	Green	0.107
D8	-4.812	-12.837	Green	Green	Green	Green	0.193
D9	-4.073	-3.003	Green	Green	Green	Green	0.353

Tables 3-4

Tables 3-4 are available in the Supplementary Files section.

Figures

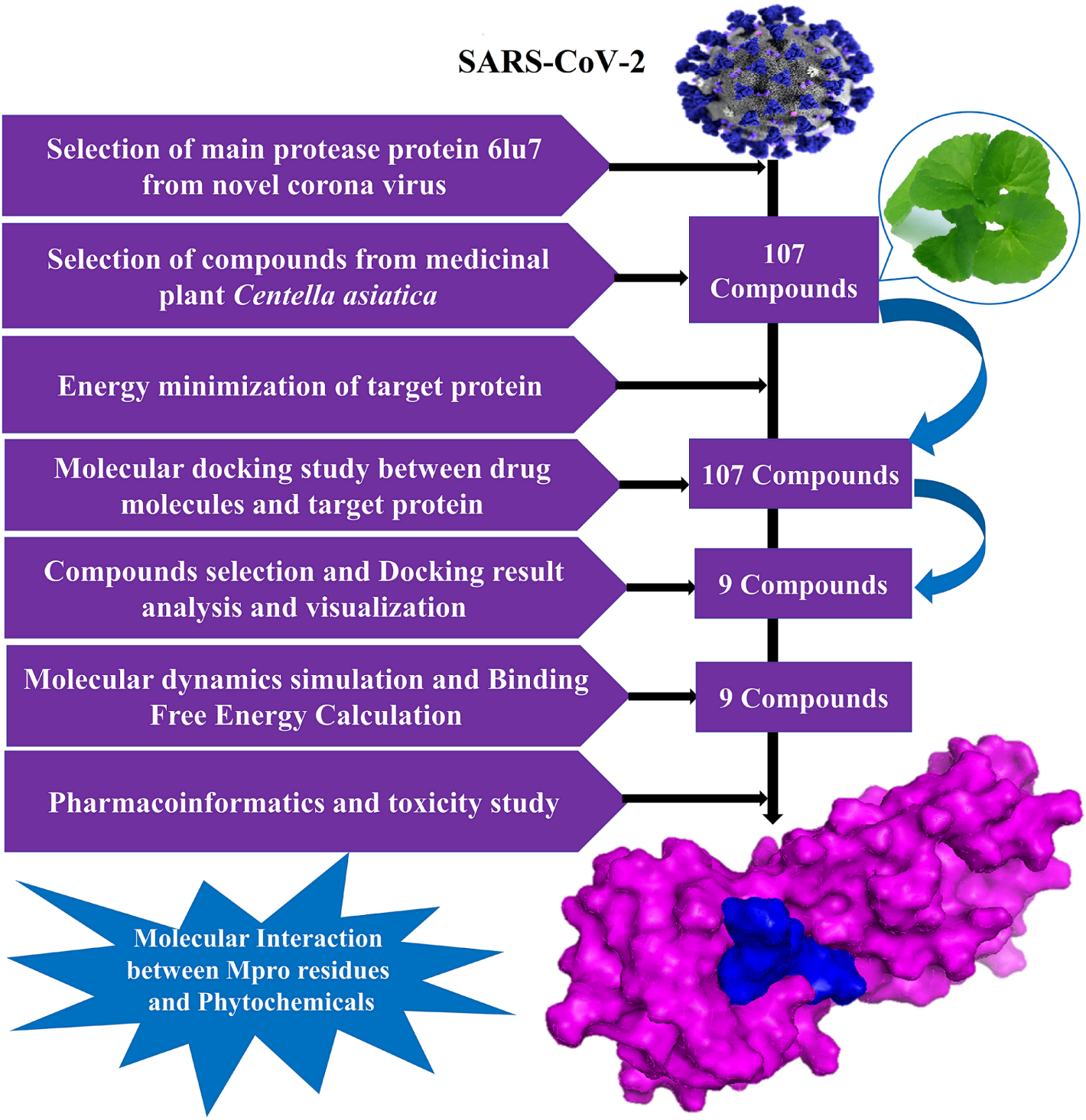

Figure 1

Flow diagram of methodologies and pipeline applied in this study.

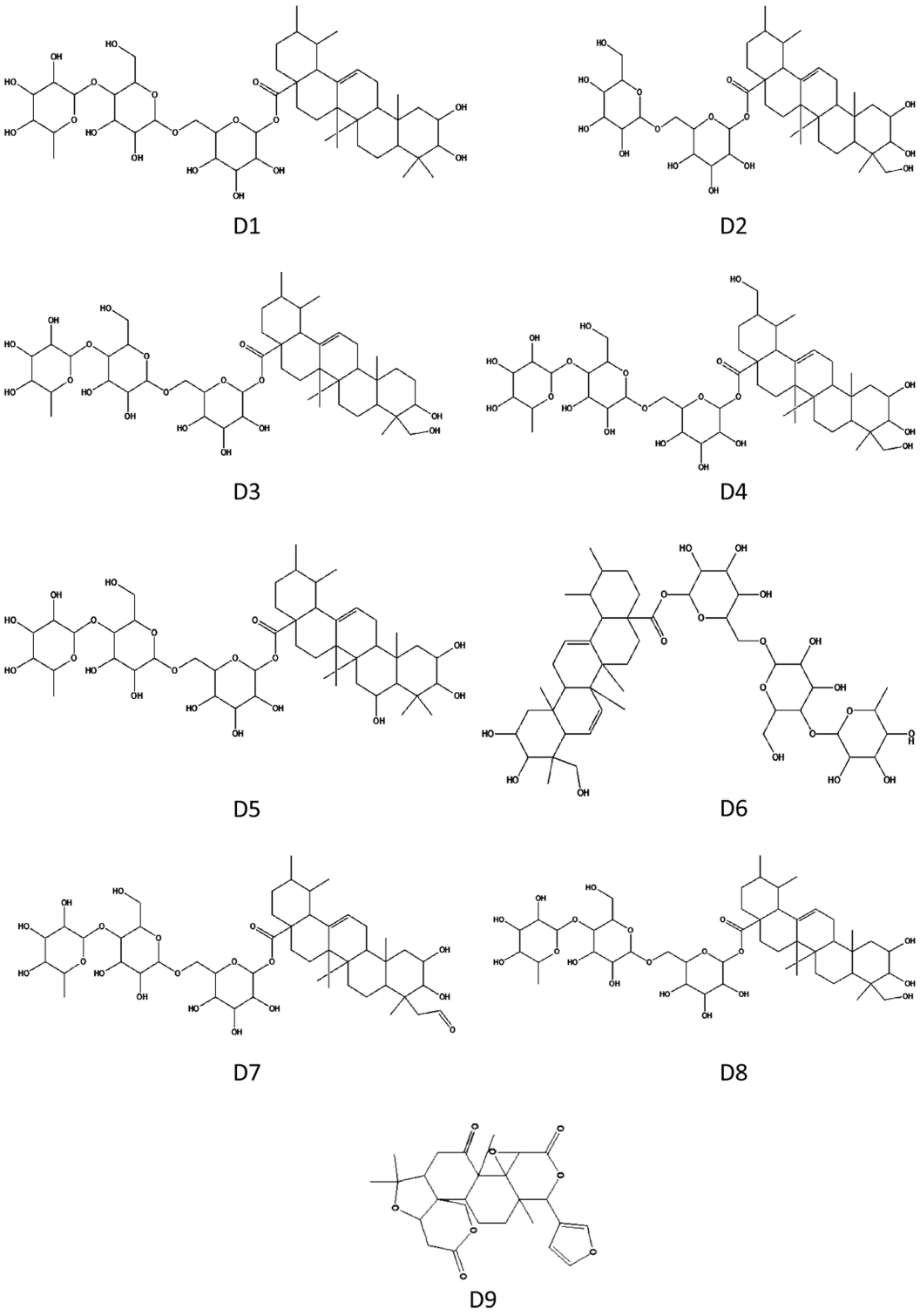

Figure 2

Chemical structure of potential bioactive phytochemicals from C. asiatica. (D1= Asiaticoside D; D2= Asiaticoside B; D3= Asiaticoside F; D4= Asiaticoside G; D5= Centellasaponin C; D6= Centelloside E; D7= Scheffuroside B; D8= Scheffuroside F; D9= Limone)

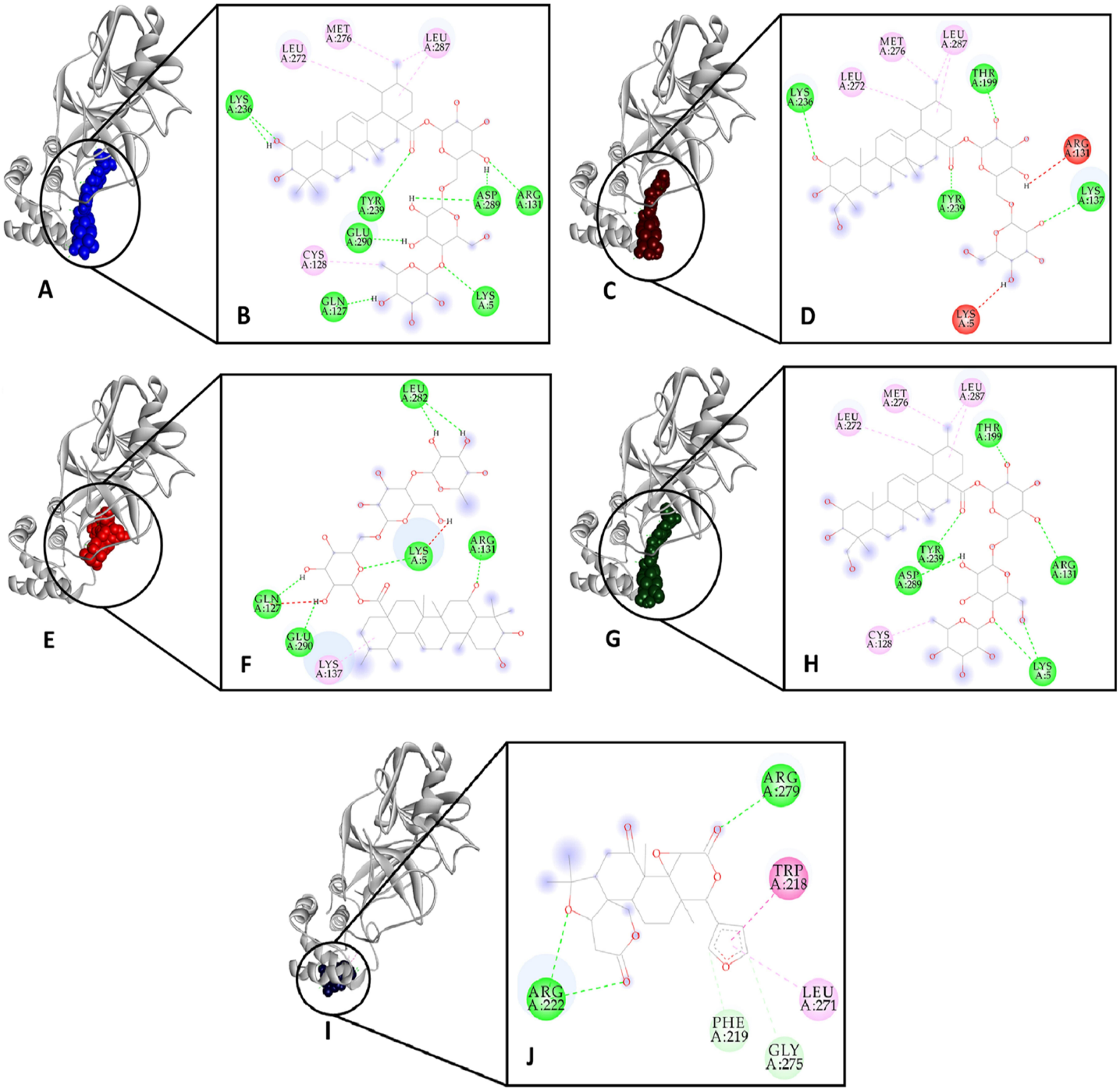

Figure 3

Three-dimensional structures are showing the binding sites of D1 (A), D2 (C), D5 (E), D8 (G) and D9 (I) in the catalytic site of Mpro, and the main residues involved in molecular interactions of D1 (B), D2 (D), D5 (F), D8 (H) and D9 (J) with the Mpro protein.

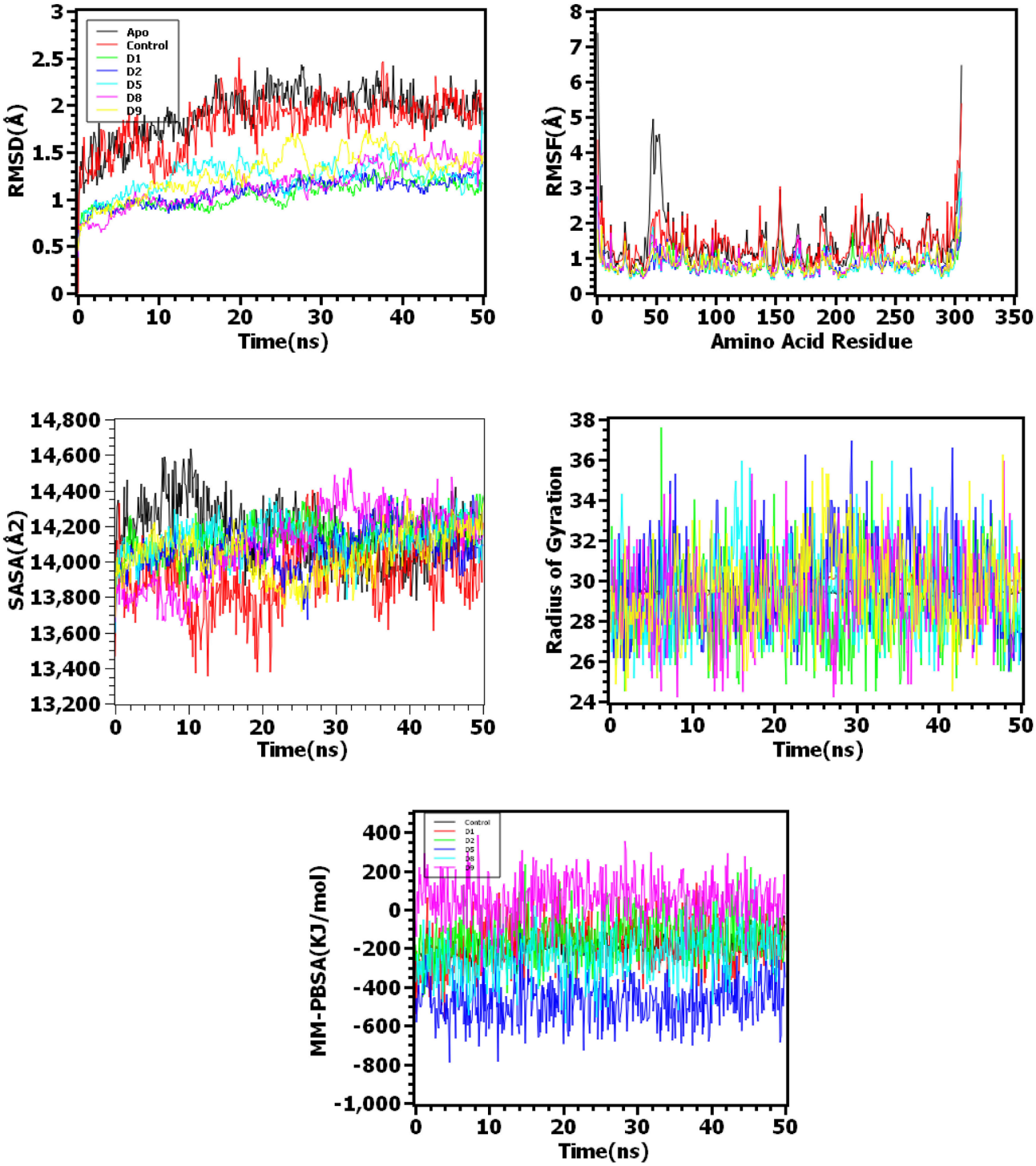

Figure 4

Molecular Dynamics Simulation and Binding Free Energy Calculation. Here, black, red, green, violet, cyan, purple, and yellow color denotes apo (without ligand), control (main protease PDB), D1, D2, D5, D8, D9 respectively.

Supplementary Files

This is a list of supplementary files associated with this preprint. Click to download.

- SupplementaryFiles.docx
- Tables34.docx
- floatimage1.png